14 HYDROGEOPHYSICAL CASE STUDIES IN THE VADOSE ZONE

JEFFREY J. DANIELS[1], BARRY ALLRED[2], ANDREW BINLEY[3], DOUGLAS LABRECQUE[4], and DAVID ALUMBAUGH[5]

[1]*Dept. Geol. Sciences, The Ohio State University, Columbus, OH, 43210*
[2]*USDA/ARS-SDRU , The Ohio State University, Columbus, OH, 43210*
[3]*Lancaster University, Department of Environmental Science, Lancaster, LA1 4YQ, UK*
[4]*Multi-Phase Technologies, LLC, Sparks Nevada*
[5]*University of Wisconsin, Madison, Wisconsin*

14.1 Overview: Detection and Monitoring in the Vadose Zone

The focus of this chapter is the characterization of the vadose zone, or the unsaturated section of the subsurface, using hydrogeophysical techniques. The regions of water saturation as they relate to the physical properties are shown for reference in Figure 14.1. Characterization below the water table (in the saturated section) is described in Chapter 13 of this volume and will not be discussed in detail here. From a physical properties perspective, the zones of variable saturation above the water table are transitional, and depend upon the soil or rock type and the lateral heterogeneity of the materials. In the vertical direction, the boundaries between all of these zones are dependent upon the types of soil, regolith, or rock that are present; the current and historical climatic conditions; and the regional and local geomorphology of the site. These same factors affect the heterogeneity of the vadose zone in the horizontal (lateral) direction and generally compound the problems of defining the different regions of moisture in the vadose zone.

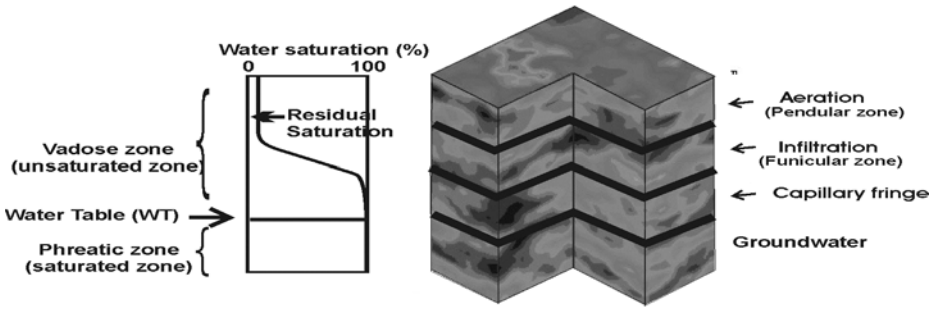

Figure 14.1. A realistic vadose zone model that emphasizes the lateral heterogeneity of the vadose zone

Y. Rubin and S.S. Hubbard (eds.), Hydrogeophysics, 413–440.

There is very little information in the literature regarding direct measurements of variations in geophysical properties (electrical conductivity, permittivity, seismic velocity, or density) in the unsaturated zone. Clearly, this is a region of fluctuations and seasonal variations in moisture content, and a region of changing geochemical regimes and bulk physical properties. Estimates of moisture within the vadose zone have primarily been studied through the use of electrical and nuclear measurements. The Topp equation (Topp et al., 1980) has been applied to measurements of the dielectric constant to obtain estimates of the moisture content, as was discussed in Chapter 4 of this volume. Estimates of dielectric constant from ground penetrating radar (GPR) have been used by several investigators to estimate water content, including Lesmes et al. (1999), Huisman et al. (2001), Huisman et al. (2003), and Grote et al. (2003). In clay-free environments, the electrical conductivity can be related to the amount of pore space occupied by fluids through Archie's law , as was also described in Chapter 4 of this volume.

Nuclear methods for estimating moisture in the near surface include the nuclear magnetic resonance (NMR) method and neutron-neutron techniques. Neutron-neutron methods are used routinely to determine the relative amount of moisture variation in the zone of aeration, but they are rarely used in a quantitative manner because of the difficulty in calibrating the instrument. NMR methods hold some promise of obtaining improved direct measurements of moisture and porosity, but field implementation of NMR is difficult, as will be discussed in Chapter 16 of this volume. Other, more common geophysical methods (magnetics, gravity, seismic, etc.) are sometimes used to determine general bulk properties of the subsurface, and to locate objects possibly associated with contaminants and the engineering aspects of the subsurface. However, these methods are not generally applicable to directly determining the hydrogeological parameters in the vadose zone.

In the past, the characterization of the vadose zone has been achieved using point measurement techniques, such as neutron probes, TDR, and tensiometry, but these methods have restricted measurement scales (typically on the order of centimeters). Since heterogeneity of the subsurface occurs at much larger scales, more appropriate measurement techniques are required. This has led to a growing interest in the use of geophysical methods for vadose zone characterization. Vadose zone hydrogeological objectives that can be facilitated using geophysical methods include: (1) defining the general hydrogeologic setting (vertical boundaries within the vadose zone), (2) determining the lateral heterogeneity of moisture content within the vadose zone, (3) monitoring and tracking infiltration through the vadose zone and into the saturated zone below the water table, and (4) locating sources of potential contamination and objects within the subsurface. In the following sections, field and experimental examples address the use of hydrogeophysical approaches for investigating these vadose zone objectives. In particular, the following case studies address some of the most fundamental problems encountered in the vadose zone: (1) estimation of hydrological boundaries, (2) soil property estimation, and (3) moisture monitoring.

14.2 Estimation of Hydrogeological Boundaries in the Vadose Zone

Determining the depth of the water table has been one of the fundamental objectives of hydrogeophysical investigations. In theory, this objective should be a simple thing to achieve with geophysical techniques, since the water table is a physical property boundary for seismic shear and compression waves, density, electrical permittivity (or the dielectric constant), and electrical conductivity (reciprocal of resistivity). The following discussion of a recent experiment that investigated the effect of moisture on the response of GPR will serve to illustrate some of the problems pertaining to interpreting geophysical measurements in terms of near-surface hydrologic properties.

A tank experiment was run at Ohio State University to determine the effect of changes in fluid levels (water and gasoline) on the GPR response. The details of this experiment were presented by Kim (2001). The tank model and experimental arrangement are shown in Figure 14.2. Fluid intake and outtake were located at the bottom of the tank to facilitate raising and lowering it without percolation of fluid from the surface. The tank was covered throughout the experiment to prevent the influx of rainwater. The overall project consisted of filling the bottom of the tank with fluid and making GPR measurements at closely spaced time intervals (approximately 30 minutes) after the water level was changed. GPR measurements were made using a GSSI SIR-10 system and a 500 MHz antenna, which was a time-domain system with co-pole antennas (parallel transmit and receive transducers) oriented perpendicular to the direction of the line traverse. Seventeen lines were run over the grid, as shown in Figure 14.2b. Consistent survey and processing parameters were maintained throughout the experiment.

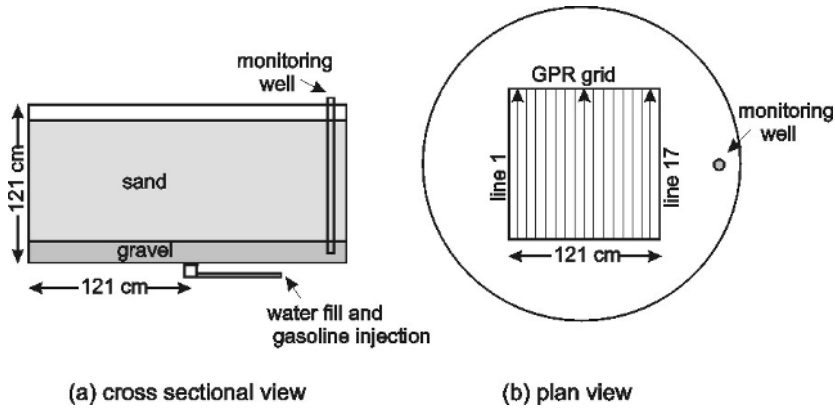

Figure 14.2. Configuration of tank and GPR survey grid in vadose zone experiment (modified from Kim, 2001): (a) cross sectional view, and (b) plan view. The porosity of the sand, gravel, and sand-gravel mix was 31%, 36%, and 11%, respectively. The capillary rise measured in the laboratory for the sand was 11.4 cm. The relative permeability for the sand, gravel, and sand-gravel interface was 7.3, 1460, and 1, respectively.

GPR 2-D profiles and 1-D traces extracted from the 2-D profiles for each monitoring stage are shown in Figure 14.3, along with the major reflection boundaries. A monitoring well inside of the tank was used to establish the water level. The water level was raised to 66 cm above the bottom of the tank in three stages (25.4 cm, 35.6 cm, and 66 cm, respectively), and subsequently was lowered in three stages (30.5 cm, 13.8 cm, and completely drained). A water level of 7.6 cm was observed in the bottom of the tank 16 hours after completely draining the tank. The residual water apparently came from residual moisture that slowly percolated down to the bottom of the tank. GPR measurements over the grid were repeated every 30 minutes to monitor changes in the GPR response. These measurements were repeated at each stage until no further changes occurred in the response on the GPR records. The stabilized results are shown for each stage in Figure 14.3. The water saturation, dielectric constant, and GPR velocity profiles determined from one-dimensional models are shown in Figure 14.4 for the 25.4 cm water level and after water drained from the tank. These models were generated using a one-dimensional modeling-program mixing model (or the complex refractive index method—CRIM; refer to Chapter 4 of this volume), which was introduced by Birchak et al. (1974) and further discussed by Wharton (1980) and Sihvola (1999).

The presence of a boundary between the zone of aeration and infiltration (refer to Figure 14.1) is not clear on the GPR records, and the GPR records (particularly the 1-D trace records) and 1-D numerical models (Figure 14.4) of the GPR data indicate that the GPR reflection interpreted as the water table actually came from the top of the capillary fringe. The capillary fringe is in tension saturation (close to 100% saturation), and it is effectively the GPR water table. The two-way travel time is nearly the same when the water was raised to the 25.4 cm level as it is when the water was lowered from 66 cm to 30.5 cm, even though the vertical distance was different. This shows that there was a significant amount of residual water in the pore space, which caused a decrease in velocity of the GPR wave after the water was drained from the tank.

Overall, the GPR data and models from this experiment indicate the stability and sensitivity of GPR measurements for determining changes in moisture above the water table. The residual water is a function of the mineralogy and the recent infiltration history of a site, and the residual water can significantly affect the velocity of the GPR wave. These measurements also show the complexity of interpreting the water table boundary from GPR data. The water table determined from GPR measurements is usually not the true hydrologic water table, but it is likely to be the upper boundary of the capillary fringe, which is close to 100% saturation. The ability to detect any hydrologic boundary on GPR records is highly dependent on the complexity of the local geology.

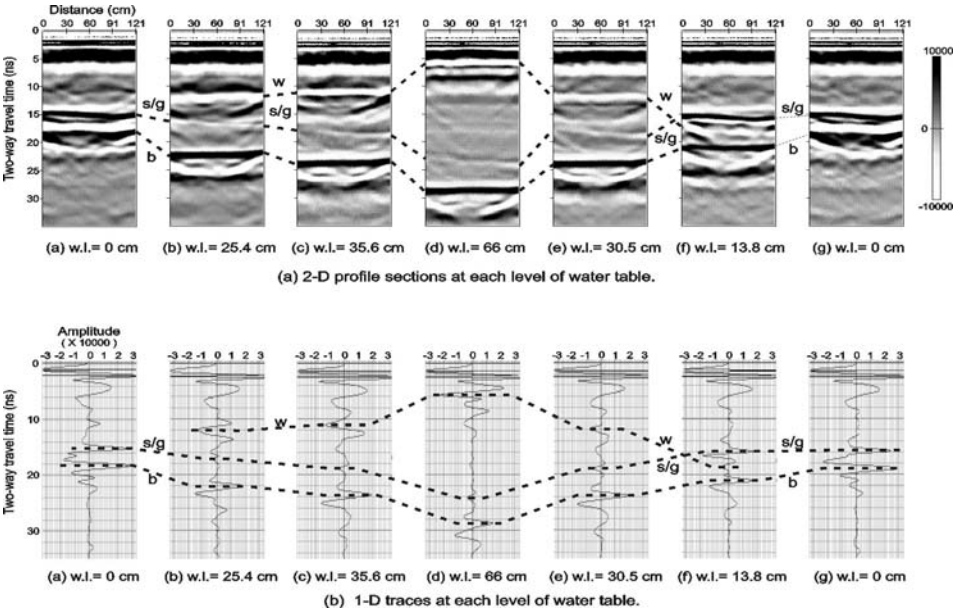

Figure 14.3. 2-D profile lines and 1-D traces after each change in the water level (modified from Kim, 2001) Water levels (wl) are given as elevation above the bottom of the tank. The water table reflection, the reflection from the sand/gravel boundary, and the reflection from the bottom of the tank are indicated by the symbols "w," "s/g," and "b," respectively.

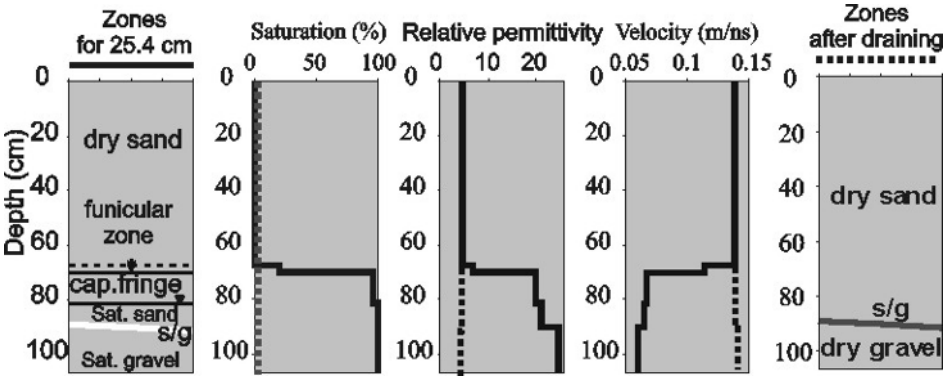

Figure 14.4. Hydrogeologic zones, water saturation, dielectric permittivity, and GPR velocity with depth at water level of 25.4 cm and after draining. The boundaries were obtained from 1-D modeling using the complex refractive index method (CRIM), as described by Wharton et al. (1980), to calculate the relative dielectric permittivity and the interval velocity of each hydrogeologic layer for a three-phase mixture of sand (quartz at a permittivity of 7 and feldspar assigned a relative permittivity of 7.5), water (relative permittivity of 80), and air (relative permittivity of 1). The sand-gravel interface is indicated by s/g. (modified from Kim, 2001).

14.3 Soil Property Estimation

The use of geophysical methods for providing hydrogeological property estimates in the vadose zone have received increased attention over the past few years for various applications—as ecological, environmental, engineering, and agricultural studies require denser and more precise estimates of soil and pore fluid properties. Near-surface geophysical methods, particularly those capable of mapping soil electrical conductivity and dielectric constant, have been used to estimate soil moisture and salinity. We review some of these studies in this section.

A substantial amount of study to date has focused on demonstrating that electromagnetic apparent conductivity (ECa) mapping is an effective tool to gauge the magnitude and spatial variability of soil salinity (Lesch et al., 1992; Hendrickx et al., 1992; Doolittle et al., 2001). Research results are mixed concerning the value of using ECa geophysical measurement techniques to monitor soil moisture. Scanlon et al. (1999) evaluated ECa measured with electromagnetic induction methods (EMI) as a reconnaissance technique to characterize unsaturated flow in an arid setting, and determined that the magnitude of the impact of moisture content on ECa was dependent on the geomorphic setting. An investigation conducted by Sheets and Hendrickx (1995) in an arid region of southern New Mexico discovered that a linear relationship existed between ECa and moisture content in the top 1.5 m of the soil profile. However, in a field study near Quebec City, Canada, carried out with traditional resistivity methods, Banton et al. (1997) found that the ECa mean and spatial patterns did not change significantly between wet and dry soil conditions. The study by Banton et al. (1997) also determined that ECa was moderately correlated with soil texture and organic matter, but not with porosity, bulk density, or hydraulic conductivity. Doolittle et al. (1994) determined a way to estimate clay pan depths in a Missouri soil, based on ECa values obtained with EMI methods. Furthermore, Fraisse et al. (2001) were able to define claypan soil management zones with a combination of topographic elevation and electromagnetic induction (EMI) ECa data. Kravchenko et al. (2002) likewise employed this combination of topographic elevation and ECa (obtained from pulled electrode array resistivity methods) to map soil drainage classes. Inman et al. (2002) found that using EMI ECa and GPR data can be a promising approach to soil surveying. Jaynes et al. (1995) estimated herbicide partition coefficients based on EMI ECa measurements. In addition, Eigenberg and Nienaber (1998) established that EMI ECa could be used as a way to detect field areas with high soil nutrient buildup. Consequently, a continually growing body of research is discovering new, potentially valuable agricultural applications for ECa mapping. Many of these studies may apply to other soil investigations.

As is apparent from this discussion of prior research, soil electrical conductivity can be affected by a number of different factors, some of which are more dominant than others depending on location, climate, etc. These factors include the soil type as determined by the mineralogy, chemistry, and grain distribution. The live vegetation can also impact the electrical property values. Electrical methods alone will not provide all of the answers for soil property analysis, but in many cases they can provide a relative indication of variations in the basic properties of salinity and moisture as a function of time and space. The following examples illustrate some of these applications.

14.3.1 EFFECT OF VARYING THE WATER TABLE ON CONDUCTIVITY

A recent investigation focused on determining the relative impact on apparent soil electrical conductivity (ECa) resulting from soil profile properties versus the factors associated with agricultural field operations or rainfall. EMI surveys were conducted under various field conditions, including different controlled shallow water table depths, changes in surface moisture content caused by rainfall or sprinkler irrigation, before and after fertilizer application and before and after tillage operations. This portion of the project took place at a test plot located behind the Ohio State University (OSU) ElectroScience Laboratory (ESL) in Columbus, Ohio (Figure 14.5). A subsurface drainage pipe system with two riser pipes connected up to the surface was installed at the site, allowing a shallow water table to be maintained at any desired level. The EMI ECa measurements for this part of the study were collected along lines oriented north-south, separated from one another by 1.5 m.

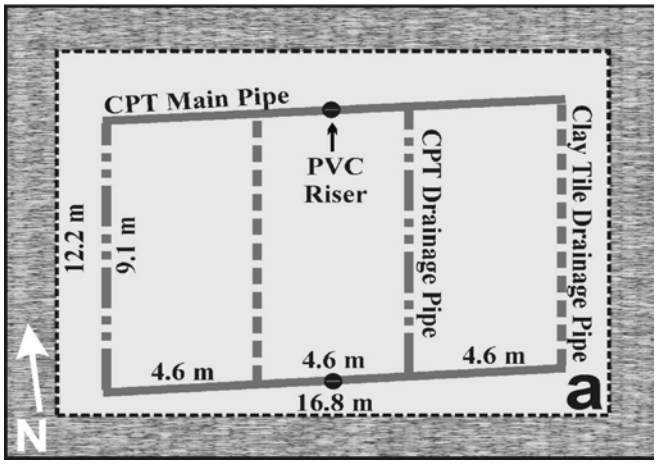

Figure 14.5. ESL #1 test plot schematic

Field conditions at the test plot utilized in this research project were monitored with water table observation wells, a time-domain reflectometry device for measuring soil surface moisture content, soil thermometers, an infrared thermometer for aboveground readings, and rain gauges. The type of soil present was a silty clay. A summary of test plot field conditions and corresponding geophysical survey results for the project are provided in Allred et al. (2003). The summary results presented in Table 14.1 for the ESL site are briefly described herein.

EMI apparent soil electrical conductivity ECa results were quite similar regardless of instrument frequency; therefore, our discussion will concentrate on data obtained at 14610 Hz using a GEM II electromagnetic induction system. Contour plots of electrical conductivity during the raising of the water table are shown in Figure 14.6. The shallow hydrologic-condition impacts were assessed through a linear regression analysis between average ECa versus average water table depth, and average ECa versus average soil surface

volumetric moisture content. The ESL #1 test area EMI survey data incorporated into this statistical analysis included data obtained on days when there was sufficient water table or soil surface moisture information available. The coeffiecient of determination from linear regression analysis (R^2) for ECa versus water table depth was 0.00, and for ECa versus soil surface volumetric moisture content, it was 0.67. Although the correlation between ECa and soil surface moisture is definitely significant, it is probably not strong enough to warrant using ECa as a direct predictor of volumetric moisture content at the ground surface. This same ECa data exhibited only minor correlation to either soil temperature (R^2 = 0.15) or air temperature (R^2 = 0.09).

Table 14.1. ESL #1 field conditions and EMI results for the part of the project focused on determining the relative impacts on ECa due to soil profile properties versus factors associated with raising the water table. ECa values are in mS/m.

DATE	**CONDITIONS**	**RESULTS (Volts × 10^{-3})**	
		Mean ECa	St Dev ECa
11/14/01	Test plot covered by tarp for previous 6 weeks. Water table > 1 m.	14.16	3.09
11/16/01	Similar to Nov. 14	13.77	2.98
07/08/02	Site stable for 7 months. Water table > 0.91 m. Mean surface soil volumetric moisture content = 20.2 %	10.4	1.65
07/ 12/02	Subirrigation with water applied through the north riser intake pipe. Water level maintained with a Hudson valve. Mean water table depth = 0.84 m, Mean soil surface volumetric moisture content = 23.0%.	7.37	1.75
07/15/02	Subirrigation continued. Mean water table depth = 0.62 m, Mean soil surface volumetric moisture content = 22.7%.	8.98	2.16
07/18/02	Subirrigation continued. Mean water table depth = 0.35 m, Mean soil surface volumetric moisture content = 41.8%.	10.36	2.86
07/19/02	Subirrigation continued. Mean water table depth = 0.27 m, Mean soil surface volumetric moisture content = 52.1%.	13.33	2.87
07/26/02	Subirrigation had been discontinued seven days prior to this date. Mean water table depth = 0.78 m	13.8	2.6
08/7/02	Subirrigation had been discontinued 19 days prior to this time	13.49	2.51
09/8/02	As a supplement to the 45.5 kg of fertilizer already applied, 22.7 kg of 21-28-7 starter fertilizer were added to the test plot eight days before this date and test plot evenly watered. Mean water table depth =0.87 m. Mean soil volumetric moisture = 29.2%.	13.15	2.38

This ECa spatial-pattern consistency, evident regardless of the field conditions, is a strong indication that soil profile properties tend to dominate the ECa response measured by near-surface geophysical methods. Higher ECa numbers are found within a tongue-shaped area that extends westward from the east boundary for almost three quarters of the test plot length. On July 19, 2002, the water table was mounded to the surface over the central portion of the test plot directly above the subsurface drainage pipe system (compare Figure 14.5 and Figure 14.6), while along the periphery of the ESL #1 test area, with the exception of the southeast corner, the soil surface was dry and the water table much lower.

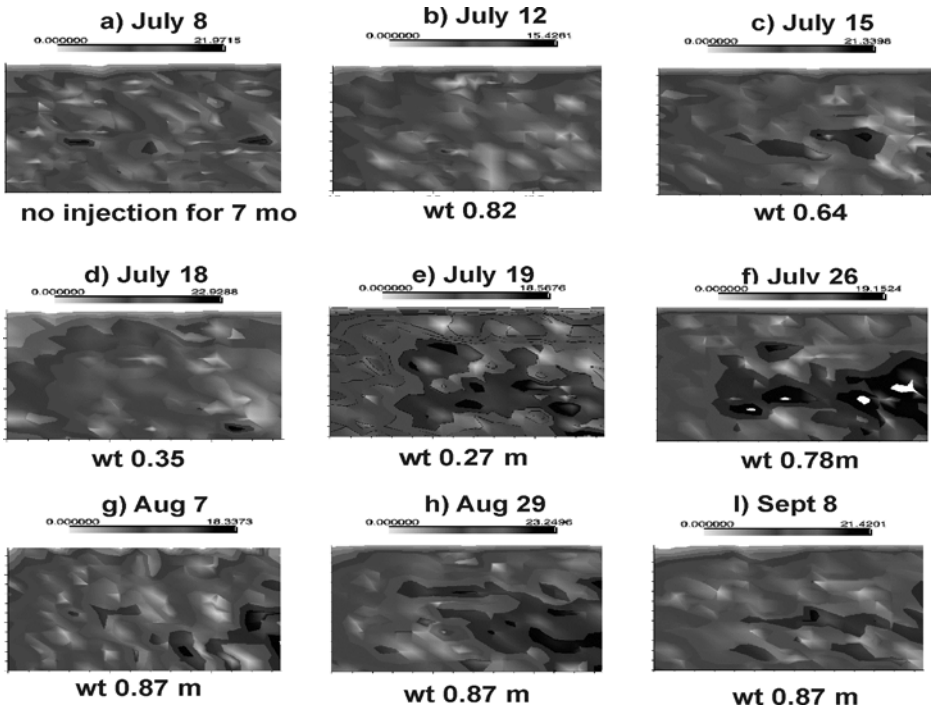

Figure 14.6. ECa contour maps for (a) July 8, 2002, (b) July 12, 2002, (c) July 15, 2002, (d) July 18, 2002, (e) July 19, 2002, (f) July 26, 2002, (g) August 7, 2002, (h) August 29, 2002, (I) September 8, 2002. Water table measurements were not taken on August 7 and August 29. Lighter colors are lower conductivity, and darker colors represent higher values of electrical conductivity.

14.3.2 ESTIMATION OF VOLUMETRIC WATER CONTENT USING SURFACE GPR GROUNDWAVE TECHNIQUES

Several recent studies have investigated the accuracy and resolution of using GPR groundwave travel-time measurements to estimate near-surface soil water content; the use of groundwave, reflected, and transmitted GPR arrivals for estimating soil water content was recently reviewed by Huisman et al. (2003b).

The groundwave is the part of the radiated energy that travels between the transmitter and receiver through the top of the soil. Advantages of the groundwave approach over

conventional approaches (GPR reflection approaches such as those discussed in Section 14.1) is that the groundwave does not require the presence of reflecting horizons or calibration information, such as the depth to a reflector, to interpret the groundwave travel time in terms of water content. As such, it has the potential to provide very-high-resolution estimates of shallow soil water content in a relatively straightforward way and in a completely noninvasive manner. Although limited to the very-near-surface soil layer, the depth sampled by the GPR groundwaves is often the critical zone for many engineering, ecological, agricultural, and environmental studies.

Using the known distance between the transmitting and receiving antenna and the measured signal travel time, the GPR velocity can be calculated and converted to dielectric constant, as was discussed in Chapter 7 of this volume. Using a petrophysical relationship between dielectric constant and volumetric water content, either developed for the particular study site or borrowed from literature (such as Topp's Equation [Topp et al., 1980]), the dielectric constant values obtained from GPR groundwave data can be used to estimate near-surface water content. Two different acquisition modes can be used to obtain dielectric constant from surface GPR data: common midpoint (CMP) or common (or single) offset, both of which are described in Chapter 7. Both Huisman et al. (2001) and Grote et al. (2003) reported that water-content estimates, from GPR groundwave CMP data, agreed well with colocated TDR estimates of volumetric water content. Huisman et al. (2001) reported a volumetric water-content accuracy of 0.024 m^3m^{-3} using 225 Mhz antennas, and Grote et al. (2003) reported root mean squared errors of the GPR-obtained volumetric water-content estimates of 0.022 and 0.015 m^3m^{-3} using 450 and 900 MHz antennas, respectively.

However, multi-offset GPR acquisition is cumbersome and time consuming, and thus not well suited for rapid estimation of water content at the field scale. As mentioned above, dielectric constant can also be obtained using common-offset GPR acquisition approaches, provided that the approximate arrival time of the groundwave is known from a multi-offset GPR measurement. The idea of using GPR groundwave data collected using the quick common-offset acquisition geometry was first suggested by Du (1996). Recent experiments by Lesmes et al. (1999), Hubbard et al. (2002), Huisman et al. (2002), Huisman et al. (2003a), and Grote et al. (2003) have confirmed that soil-water-content estimation using common-offset groundwave travel-time data is a viable approach for quickly providing soil-water-content estimates at the field scale. In an irrigation experiment, Huisman et al. (2002) used 225 MHz common-offset GPR groundwave data to estimate soil water content over a 60 × 60 m area and found that the GPR estimates agreed very well with those measurements obtained using conventional TDR methods, but that the GPR approach provided much-higher-resolution information in a noninvasive manner.

Using 450 and 900 MHz common offset GPR groundwave data, Grote et al. (2003) estimated the spatial and temporal variations in near-surface water content over a large-scale agricultural site during the course of a year. They found that soil texture exerted an influence on the spatial distribution of water content over the field site. In addition, although the mean values of water content varied as a function of season and precipitation, the spatial pattern of moisture content within the natural field was temporally persistent. Compared with soil sample gravimetric measurements of water content, they reported a

root mean squared error of 0.011 for the 900 MHz data and 0.017 for the 450 MHz data using the common-offset GPR groundwave approach.

Figure 14.7 illustrates a time series of volumetric water-content estimates obtained at a California winery study site using 900 MHz surface common offset GPR data (modified from Hubbard et al., 2002). Each image in this figure includes over 20,000 estimates of volumetric water content obtained using GPR data, and although the absolute estimates of water content change with time, the spatial pattern clearly remains the same.

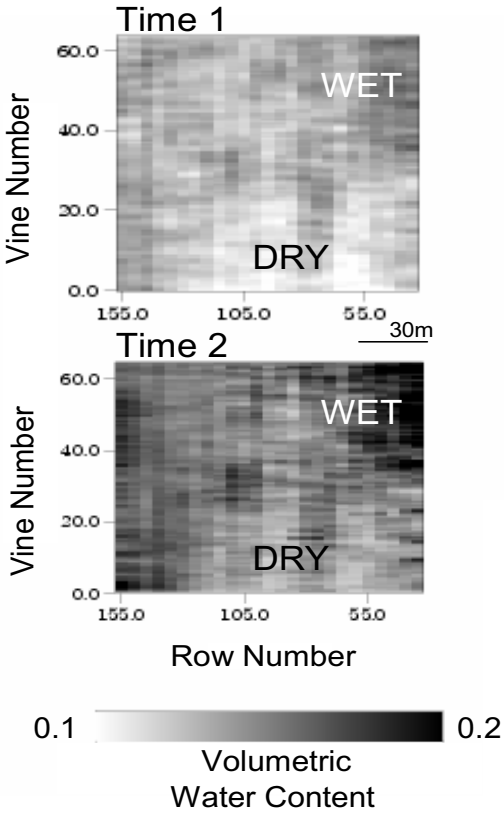

Figure 14.7. Soil moisture estimated over a winery study site using surface 900 MHz GPR groundwave data at various times during the year. Each image = ~20,000 data points. Modified from Hubbard et al. (2002).

The effective measurement volume of the GPR groundwave is still a topic of research. Huisman et al. (2001) concluded that soil-water-content measurements based on groundwave data are similar to measurements with 0.10 m long TDR probes for both the 225 MHz and 450 MHz GPR antennas. Grote et al. (2003) compared estimates of water content obtained using 450 MHz and 900 MHz common-offset GPR groundwave data with measurements collected using gravimetric techniques, in soils having various textures and at depths between 0 and 0.10 m, 0.10 and 0.20 m, and 0 and 0.20 m below ground surface. They found that the estimates obtained using these frequencies showed the highest

correlation with the soil-water-content values averaged over the 0–0.20 m range and the least correlation with the water-content measurements taken from the 0.10–0.20 m interval.

As described by Huisman et al. (2003b), there are some drawbacks to using the GPR groundwave to estimate soil water content. These drawbacks include the potential difficulties associated with: (1) clearly distinguishing the groundwave from other arrivals, (2) choosing an antenna separation for which the arrival times of the air and groundwave can consistently be picked, despite moving the antennas across a field with varying soil water content, and (3) collecting groundwave data at far antenna separations, (since the groundwave is attenuated more quickly than other waves.) In spite of these potential limitations, GPR groundwave travel-time data have provided accurate, very-high-resolution estimates of shallow soil water content.

14.4 Moisture Monitoring in the Vadose Zone Using Resistivity

Because electrical resistivity is a volumetric measurement of volumetric moisture content (see Chapter 4 of this volume), resistivity surveys have proven to be of great value in aiding hydrological studies of the vadose zone. Most previous applications have concentrated on monitoring forced loading of the system via tracer tests (see, for example, Section 14.5 below). Few studies, however, have used resistivity methods to examine changes in moisture content of soils caused by natural loading. The focus here is on examples of how resistivity has been used to study such conditions.

Several investigations of vadose zone processes have used surface-deployed resistivity surveys for monitoring moisture. Kean et al. (1987) described the use of vertical electrical soundings (VES; see Chapter 5 of this volume) for studying changes in the vadose zone under natural loading. At one of their survey sites, Kean et al. (1987) observed changes over a 10-week period, albeit in a shallow water table environment. Frohlich and Parke (1989) also used VES to infer changes in moisture content in the unsaturated zone. In their case, measurements were made over a period of 9 weeks; changes in resistivity to the water table depth (approximately 3 m) were observed and compared with the conventional neutron probe measurements.

Surveys based on VES are somewhat limited, given the non-uniqueness of inversion methods for soundings (as demonstrated, for example, by Simms and Morgan, 1992). Perhaps more restrictive is that the measurement volume (lateral and vertical variations) for soundings increases with depth. This will create significant errors if any lateral variability in resistivity exists (caused by lithology and/or moisture content). Benderitter and Schott (1999) have shown how surface resistivity surveys can be used to reveal such lateral variability, by analyzing changes in moisture content during rainfall events over a 100-day period. Benderitter and Schott used a short (7.5 m) traverse with 15 electrodes and measured apparent resistivity using a dipole-dipole configuration (see Chapter 5 of this volume). Consequently, the depth of sensitivity for their surveys was limited to the top meter. In a more recent study, Zhou et al. (2001) used a combined surface-borehole electrode array to map natural changes in resistivity caused by rainfall inputs. In their investigation, only short-duration events (several days) and near-surface (top 1.5 m)

changes were studied. Zhou et al. (2001) claim that their approach, at their site, is capable of measuring moisture contents with 0.1 m^3 m^{-3} errors, although changes in moisture content should be more accurately resolved.

Two other examples are presented here, in which the resistivity method has been used to study changes in moisture content within the vadose zone under natural loading. In the first case study, surface resistivity arrays are used to monitor the spatial variability of infiltration resulting from snowmelt in a small field plot in Norway. In the second case study, borehole electrode arrays are utilized to monitor small moisture-content changes to a depth of 10 m at a sandstone aquifer in the U.K.

14.4.1 MONITORING SNOWMELT USING SURFACE ELECTRICAL METHODS

Experiments have been carried out in Norway to study flow and transport processes during snowmelt. The experiments were driven by the need to determine rate estimates for transport and retardation of pollutants from diffuse source pollutants, such as de-icing chemicals. At the Morreppen field site, adjacent to Oslo Airport, an extensive series of hydrological and biogeochemical investigations were completed, and a series of geophysical surveys were taken during 2001 to supplement earlier studies. French et al. (2002) report results from cross-borehole electrical resistivity surveys, designed to monitor the movement of salt tracers applied beneath the snow cover. The results from French et al. (2002) support earlier observations of preferential transport through the sand and gravel sediments in the vadose zone. The following case study summarizes results from surface resistivity surveys carried out during the snowmelt period of 2001. These surveys were performed to assess the spatial variability of infiltration caused by snowmelt, and thus determine the validity of assuming diffuse sources within any predictive hydrological model applied at the site.

Figure 14.8 illustrates the change in groundwater level during the 2001 snowmelt period, when the response of the water table to onset of snowmelt during April 2001 was rapid.

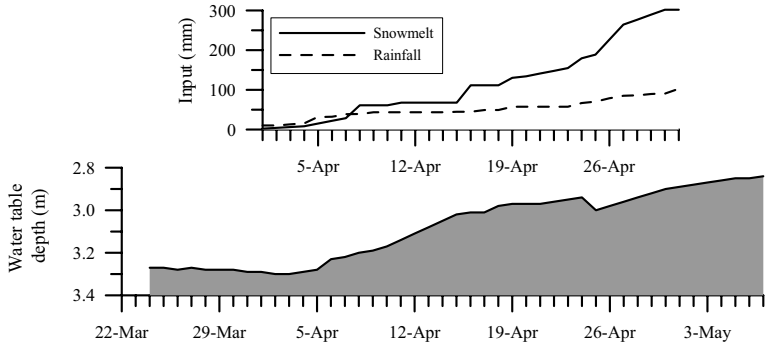

Figure 14.8. Cumulative inputs during snowmelt period in 2001 at the Moreppen field site and measured water table depth

During 2000, to determine the spatial variability of infiltration, investigators installed 80 electrodes at 0.2 m depth (to avoid near-surface ground-frost effects) in a small field plot 1 m wide by 3.75 m long. The electrodes were arranged in a grid at 0.25 m spacing. Using a Wenner configuration (see Chapter 5 of this volume), investigators carried out electrical resistivity surveys prior to snowmelt and during the snowmelt period. The data were inverted using a 3-D inverse model to produce images of resistivity (to a depth of 0.6 m) during the snowmelt event.

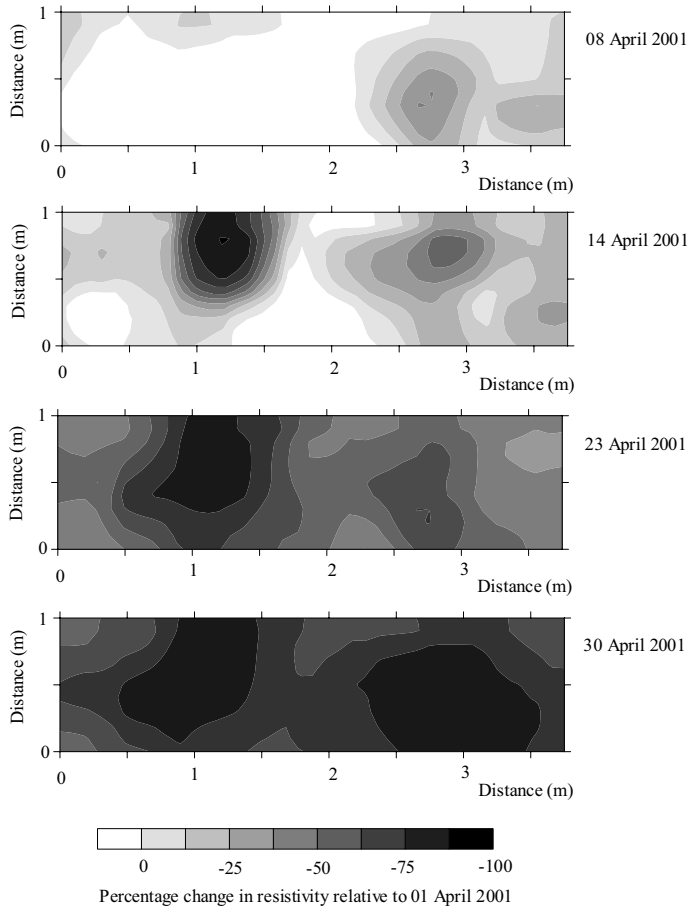

Figure 14.9. Changes in resistivity at the ground surface due to snowmelt at the Moreppen field site

Figure 14.9 shows a selection of results from the resistivity survey. Here, changes in resistivity relative to April 1, 2001, are shown for the horizontal plane corresponding to the top 0.1 m of the soil profile. The images reveal significant localized changes in resistivity during the initial phase of the snowmelt event, suggesting preferential infiltration. Towards the end of the event, more widespread infiltration appears to exist. The observed response is likely to be a result of localized thawing of the near-surface soil horizon. Prior to any

such thaw, the soil surface impedes any infiltration. Note that significant changes in resistivity are observed, as a result of intensive loading on an initially dry soil. The results from the geophysical survey support a hypothesis that preferential infiltration occurs at the site. These findings must be considered alongside evidence of preferential transport in deeper soil sections and will hopefully lead to the development of more appropriate regulatory models of flow and transport at the site.

14.4.2 MONITORING SEASONAL CHANGES IN SOIL MOISTURE USING BOREHOLE ELECTRICAL METHODS

Given the limited depth sensitivity of surface resistivity surveys, Binley et al. (2002) demonstrated how borehole-based electrode arrays may be used to characterize seasonal variation in moisture content to depths of 10 m at a sandstone site in the UK. This study supplemented earlier work using borehole radar tomographic methods to determine changes in moisture content caused by forced (tracer) and natural hydraulic loading at the site (Binley et al., 2001). The study of seasonal variation by Binley et al. (2002) was carried out over two years, allowing comparison of changes with estimated net rainfall inputs.

For the study by Binley et al. (2002), electrical resistivity tomography (ERT) surveys (see Chapter 5 in this volume) from a 32-electrode array in a single borehole were converted to vertical resistivity profiles using data inversion techniques, by discretizing the vertical profile into 0.82 m thick units. Using site-specific petrophysical relationships between moisture content and resistivity, these electrical profiles were converted to moisture content profiles. Figure 14.10 shows example results from the work of Binley et al. (2002). In Figure 14.10, the monthly net rainfall at the site between July 1998 and November 2000 is shown. Changes in the bulk electrical conductivity for the near-surface unit (i.e., representing the top 0.82 m soil zone) are shown in Figure 14.10b. The correlation between electrical conductivity and net rainfall amounts is clearly seen. Figure 14.10c reveals changes in moisture content estimated from electrical conductivity throughout the unsaturated sandstone profile (2 to 10 m depth). The delay in response owing to the winter wetting periods, caused by the hydraulic impedance of the near-surface sediments, is seen to be several months. Once the sandstone responds to such inputs, migration through the profile to a depth of 6 to 7 m is rapid. Hydraulic resistance at this depth is then apparent from the step change in moisture content with depth. (Notice how small the increase is in moisture content at depths beyond 7 m during March and April 1999, despite continual increases at shallower depths.) The inferred hydraulic resistance is consistent with the observed location of fine-grained sandstone recorded from cores taken from the site. Further note, in Figure 14.10c, that the drying fronts are also visible to significant depths in the profile. The small moisture-content changes at depth inferred from these surveys could not be inferred from surface-deployed resistivity arrays.

Binley et al. (2002) also compared moisture-content changes inferred from electrical resistivity to those derived from borehole radar profiles—and demonstrated consistency in their responses. Binley and Beven (2003) used these data to examine the potential to calibrate hydraulic flow models for the site, with the aim of using geophysical data to constrain predictions of pollutant transport through the vadose zone.

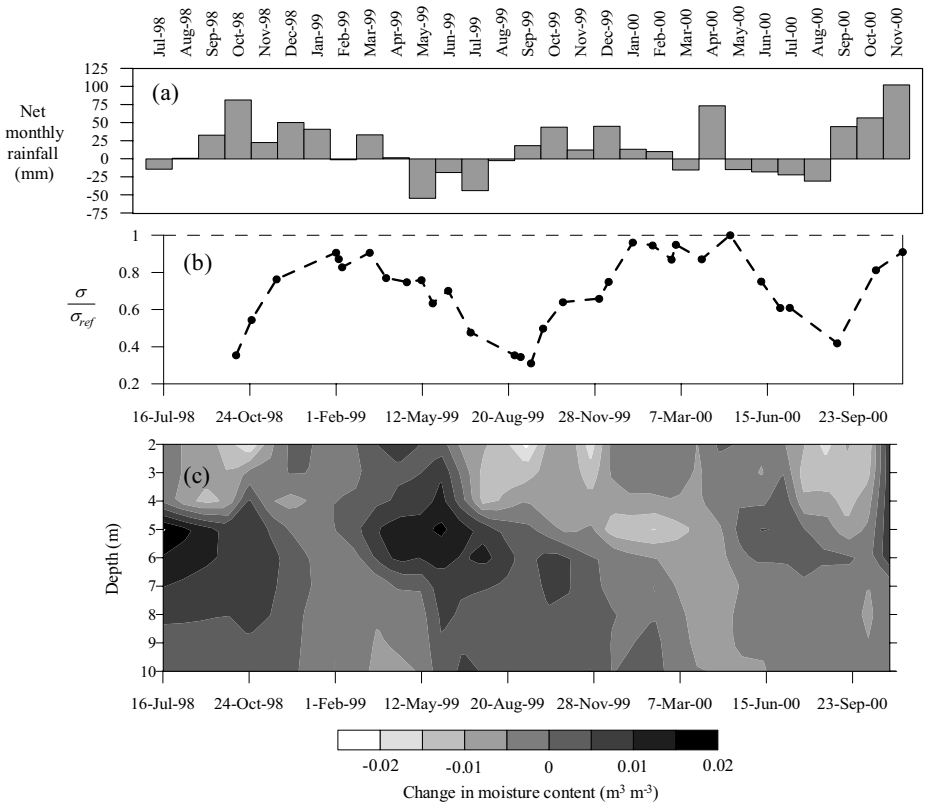

Figure 14.10. (a) Net monthly rainfall estimates at the Hatfield site (supplied courtesy of the UK Environment Agency); (b) fractional change in bulk electrical conductivity in 0–0.82 m layer relative to May 3, 2000; (c) change in moisture content throughout unsaturated zone (values computed relative to February 1, 1999)

14.5 Monitoring Forced Infiltration at a Single Site Using Multiple Methods

The Sandia/Tech vadose zone (STVZ) site in New Mexico was constructed to study the combined use of geophysical methods and hydrological modeling to monitor unsaturated flow processes within a heterogeneous sedimentary site. The instrumented portion of the STVZ site was approximately 10 m × 10 m (Figure 14.11) × 13 m deep. A 3 m × 3 m infiltrometer was installed at the center of the site to infiltrate water at a known, constant rate. The infiltrometer was divided into nine 1 m^2 arrays, each array containing 100 equally spaced medical needles mounted on 50 mm PVC pipes. The remainder of the test area was covered by a polyethylene tarp to create a no-flow boundary along the earth's surface. The top part of the infiltrometer was covered with insulating foam and a second polyethylene tarp to minimize evaporation or additional infiltration through the top (Paprocki, 2000).

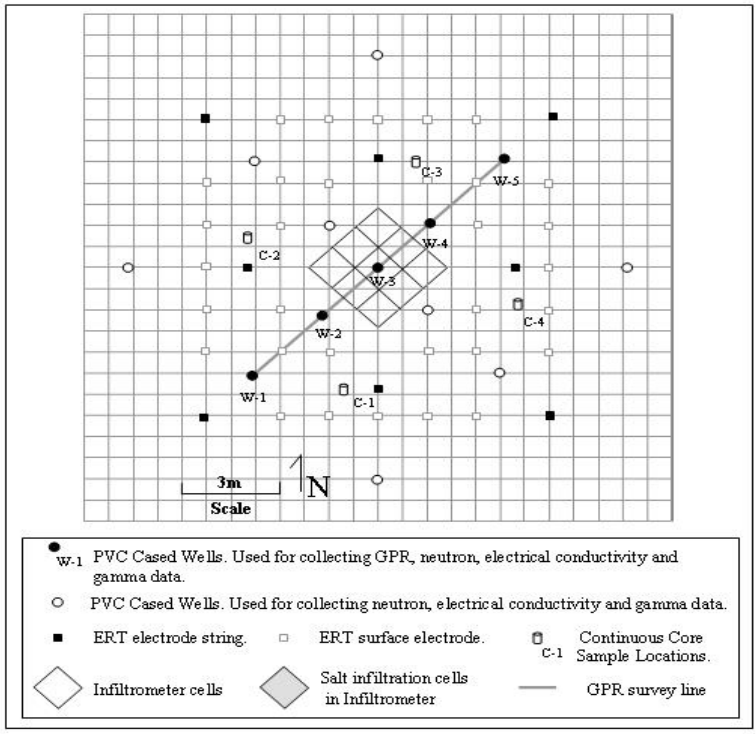

Figure 14.11. Arrangement of boreholes at the STVZ site

Site stratigraphy (Figure 14.12) was determined from four continuous core samples (see Figure 14.11). Note that the clay content of the poorly sorted gravel layer, from 4 to 7 m in depth, increased towards the northwest corner of the site. This layer had a lower hydraulic conductivity than the sand layers and served as a barrier to the downward migration of water.

Thirteen PVC-cased wells were installed at the site, with a maximum depth of 13 m. Neutron measurements and induction logs were collected along these wells. Cross-borehole ground penetrating radar (GPR) surveys were also conducted in five PVC-cased wells along an 11 m diagonal line from the southwest to the northeast end of the site (Figure 14.16). Nested time-domain reflectometry probes (TDR), tensiometers, and suction lysimeters (not shown) were placed along the outer perimeter of the infiltrometer and between the PVC-cased wells.

In addition to neutron measurements and GPR, a three-dimensional (3-D) ERT system was installed at the STVZ site to provide 3-D images of electric conductivity. The ERT system used a combination of surface and borehole electrodes. Surface electrodes consisted of 30 cm lengths of copper-plated steel rod driven into the surface of the site (Figure 14.10). Electrodes were placed in eight boreholes. Each borehole contained 17 stainless-steel

electrodes placed at 0.76 m intervals, with the uppermost electrode approximately 0.5 m below the surface.

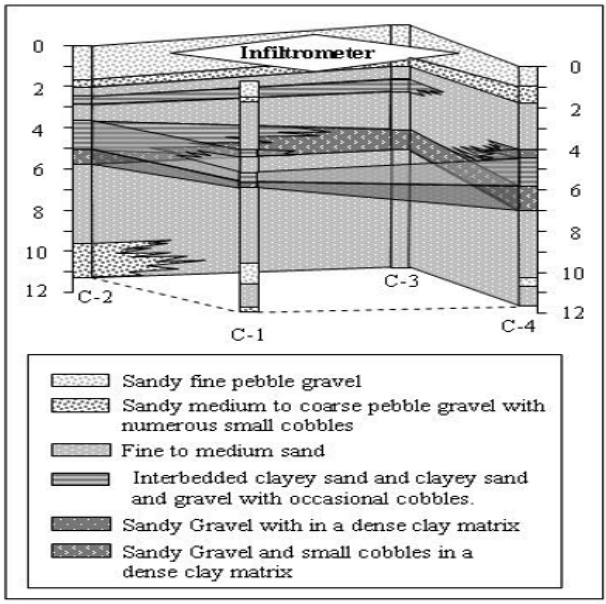

Figure 14.12. Stratigraphy of the STVZ site

14.5.1 GPR DATA COLLECTION AND PROCESSING AT THE STVZ SITE

A Sensors and Software PulseEKKO 100 system, with an antenna frequency of 100 MHz, was employed to obtain cross-borehole GPR measurements. Data were acquired by positioning the transmitting antenna within a borehole, and then collecting data at several receiver depths in another borehole 2 to 3 m away. The transmitting antenna was then moved to a new position, and data were collected in the same way. Repeating this process creates a dense array of intersecting ray paths, where each ray path represents the shortest path perpendicular to the EM wave front that passes through the region between the two boreholes. During data collection, the angle of the transmitting antenna and the receiving antenna to the horizontal was limited to 45º to avoid the influences of wave reflections from high angles of antenna offset (Peterson, 2001), low signal-to-noise ratios at high angles, and problems with the presence of wires on the ground (Paprocki, 2000; Alumbaugh, 2002). To assure that the output radar signal of the GPR system did not fluctuate during the data collection, a time-zero calibration was conducted every 10 transmitter depths. This involved placing the transmitting and receiving antennae in the air at a known distance. The correct time-zero can be determined from the travel time calculated by the speed of light in air and the known distance.

The inversion code GeotomCGTM (GeoTom, LLC, 1998) was used to produce images of velocity and attenuation from travel time and normalized amplitude measurements. GeotomCGTM is based on the simultaneous iterative reconstruction technique (Jackson and Tweeton, 1996) and uses ray tracing methods to generate tomographic images. Straight ray inversion, which assumes the ray path between the transmitter and receiver is a straight line, was chosen for both velocity and attenuation inversion. Theoretically, EM waves tend to travel through high-velocity regions rather than low-velocity regions. This makes the ray paths in an inhomogeneous media tend to curve around the low-velocity regions, and thus they are no longer straight lines. Although in theory it is more accurate to use curved-ray inversion (Alumbaugh et al., 2002), there were difficulties with the curved-ray inversion providing stable solutions for the attenuation data. Investigators chose to use the straight ray inversion because it seemed to be more robust for the attenuation tomograms in this study (see Chang et al., 2003).

The inversion code provides images of GPR velocity and attenuation on a discrete grid of cells, with an interval of 0.25 m in both the horizontal and vertical direction. The inverted images were then converted into estimated volumetric water content and electrical conductivity. Given volumetric water content, θ_v, the value of dielectric constant, k, can be estimated from the empirical relation developed for this site by Alumbaugh et al. (2003):

$$\theta_v = 0.0136\kappa - 0.033 \tag{14.1}$$

For GPR data where the frequency ω is high enough that $\omega\varepsilon >> \sigma$, the conductivity can be determined from

$$\sigma \cong 2\sqrt{\frac{\varepsilon_0}{\mu}}\sqrt{\kappa}\alpha \cong \frac{\sqrt{\kappa}}{188.5}\alpha \tag{14.2}$$

where α is attenuation in Nepers/m, σ is conductivity in S/m, ε_0 is the free-space permittivity, κ is dielectic constant, and μ is magnetic permeability.

14.5.2 ERT DATA COLLECTION AND PROCESSING STVZ SITE

The ERT data were collected using the dipole-dipole array with combinations of the vertical electrode arrays and surface electrodes. The data were collected using a system that utilized 3 receiver channels and a multiplexer capable of connecting up to 120 electrodes at a time. Reciprocal measurements were used to remove noisy data. Reciprocal pairs that differed by more than 10% of the data value were removed from the data. The remaining pairs were averaged. Typically, about 30% of the data were removed. The final averaged data sets usually contained about 20,000 points. The results presented here used the 3-D anisotropic inverse algorithm described by LaBrecque and Casale (2002). The code also implements a differencing inversion scheme similar to that described by LaBrecque and Yang (2001) to allow effective imaging of small changes in background resistivity. The region to be imaged was discretized into a mesh of $44 \times 44 \times 40$, for a total of 77,440 elements. Element size ranged from 0.38 m in the center of the mesh, to 6 m along the boundaries. The inversion of a complete background data set took about 9 hours on a Pentium 4, 1.8 GHz PC.

14.5.3 BOREHOLE LOGGING DATA AT THE STVZ SITE

Neutron measurements were collected using a Campbell Pacific Nuclear International Inc. Model 503-DR Hydroprobe. Measurements were taken at 0.25-meter intervals. The probe was calibrated by collecting TDR and neutron data simultaneously at three depths in a small pit adjacent to the test area. Prior to emplacement, the TDR probes in the pit were calibrated in the laboratory using sediments from the test area (Paprocki, 2000). The calibrated TDR data were used to create a linear calibration curve for the neutron data. The same boreholes used for neutron measurements were also logged using a Geonics EM-39 borehole induction tool at 0.25-meter intervals.

14.5.4 RESULTS OF GEOPHYSICAL SURVEYS AT THE STVZ SITE

Prior to the start of water infiltration, multiple sets of background data were completed for each of the four techniques. Starting in March 1999, fresh water with a conductivity of about 70 mS/m was infiltrated at a rate equivalent to 2.7 cm/day over the area of the 3 m × 3 m infiltrometer. It should be noted that conductivity of the background water was around 200 to 400 mS/m, somewhat higher than the infiltrating water. Although the sediments contained some buffering capability such that the salinity (and thus the conductivity) of the infiltrating water increased, this buffering capability was depleted during the coarse of the experiment. Measurements of pore-water samples taken after two years of infiltration showed that the water in the principal flow paths was close to the conductivity of the pore water. There were two competing effects during the experiment: (1) increased pore-water content, tending to increase the bulk conductivity of the soil, and (2) decreasing salinity of the pore water, tending to decrease the bulk resistivity.

14.5.4.1 *3-D ERT Results at the STVZ site*

Figure 14.13 shows 3-D views of the background conductivity distribution for ERT and the changes in conductivity at three times after the start of infiltration. In the background images, the strongly resistive zones (Figure 14.13a) have been made transparent. The images show a relatively conductive zone corresponding to the clay bearing zones between 2 and 6 m in depth.

During the early phase of infiltration (Figure 14.13b), there is a small elliptical zone of increased conductivity in the fine sands below the infiltrometer. Very little water is retained within coarse sands and gravels immediately below the infiltrometer; thus, the water moves quickly through this layer and the bulk conductivity of this layer increases only slightly from the pre-infiltration value.

After just over one month of infiltration (Figure 14.13c), the water moved downward and westward, and some of the fluid was located outside the image zone. The conductive zone was large within the finer-grained sediment layers and smaller in the intervening beds.

After a year of infiltration (Figure 14.13d), the size of the conductive zone decreased from that shown in Figure 14.13c. This apparent decrease is at least in part caused by the

removal of salts from the subsurface, such that the pore water within the zone has a lower conductivity. In addition, the water was significantly colder in March 2000. Because of the rapid infiltration, thermocouple data (not shown) from the site show annual changes in temperature as large as 18ºC at a depth of 2 m and 11ºC at 4 m. The decrease in temperature can significantly decrease the pore water electrical conductivity.

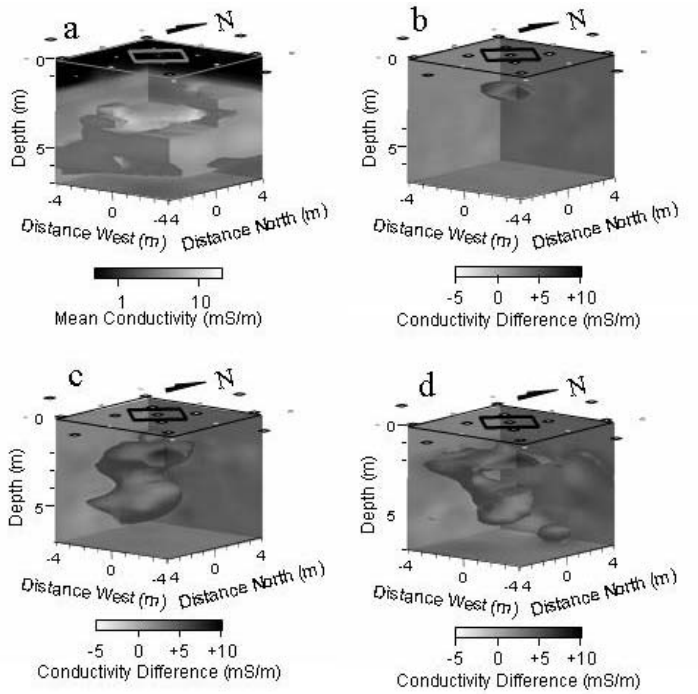

Figure 14.13. Composite showing images of 3-D ERT results of conductivity or change in conductivity for (a) pre-infiltration background data collected February 16, 1999; (b) data collected April 20, 1999, approximately 10 days after the start of infiltration, (c) data collected, March 20, 1999, approximately 40 days after the start of infiltration; and (d) data collected on March 28, 2000, approximately 1 year after the start of infiltration.

14.5.4.2 *Comparison of ERT, GPR, Neutron, and EM-39 Results*

Figure 14.14a shows an image of soil moisture content along the SW-NE profile as derived from GPR velocities. The values of moisture content estimated from calibrated borehole neutron measurements are superimposed on the GPR images. Both GPR and neutron results show water content as the percent of the total soil volume and are plotted on a scale of 0 to 10%.

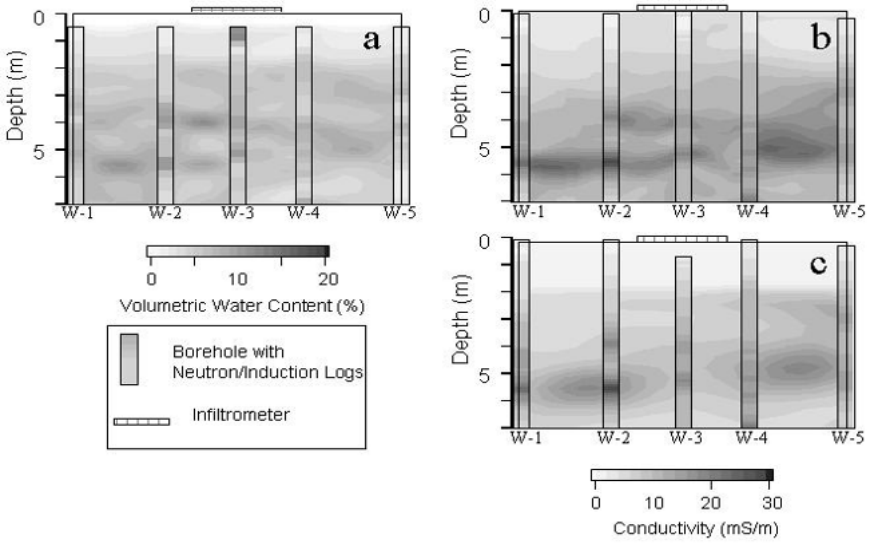

Figure 14.14. Pre-infiltration images of (a) volumetric water content from GPR and borehole neutron data; (b) conductivity data from crosshole GPR attenuation and borehole induction logs; and (c) ERT and borehole induction logs. Data were collected in February 1999.

The region of high moisture content seen at the top of the neutron log in borehole W-3 is caused by bentonite placed in the borehole annulus just below the infiltrometer. The bentonite was placed at the top of this borehole to prevent water from moving down the borehole annulus below the infiltrometer. The remaining portions of this borehole and all of the other boreholes were backfilled with native sediments. There are also some discrepancies between the radar and neutron results in the outer boreholes, particularly borehole W-1. Note that both methods have limitations, and the true moisture content probably lies somewhere between the two results. GPR images will tend to have lower resolution than neutron logs, particularly when the distance between the boreholes increase. On the other hand, the neutron data are more susceptible to near-borehole effects.

In Figure 14.14b, GPR attenuation data, obtained from GPR amplitudes, were used with the GPR dielectric information (obtained from GPR travel time data) to estimate electrical conductivity in mS/m, following Equation 14.2. Induction logging data collected using the EM-39 are superimposed on the GPR images. For most of the wells, there is very good correlation between the EM-39 results and the conductivity derived from GPR data. Although the electrical conductivity of sediments is a function of a number of factors—including clay content, pore-water salinity, and porosity—the similarities between the moisture content (Figure 14.14a) and conductivity (Figure 14.14b) indicate that conductivity and moisture content may be strongly correlated at this site.

The final panel, Figure 14.14c, shows conductivities extracted from the 3-D ERT images. Although the ERT images agree with the overall pattern seen in the GPR images, a highly resistive layer at the top and a conductive zone from 3.5 m to 6 m in depth, the ERT images have lower resolution than those of the GPR and EM-39.

After the onset of infiltration, neutron, GPR, and ERT data were collected periodically. Figures 14.15 and 14.16 compare the use of the three geophysical methods for following the infiltration front after approximately 10 days and 40 days of infiltration respectively. All of the methods show changes in volumetric moisture content or electrical conductivity from the background images shown in Figure 14.14.

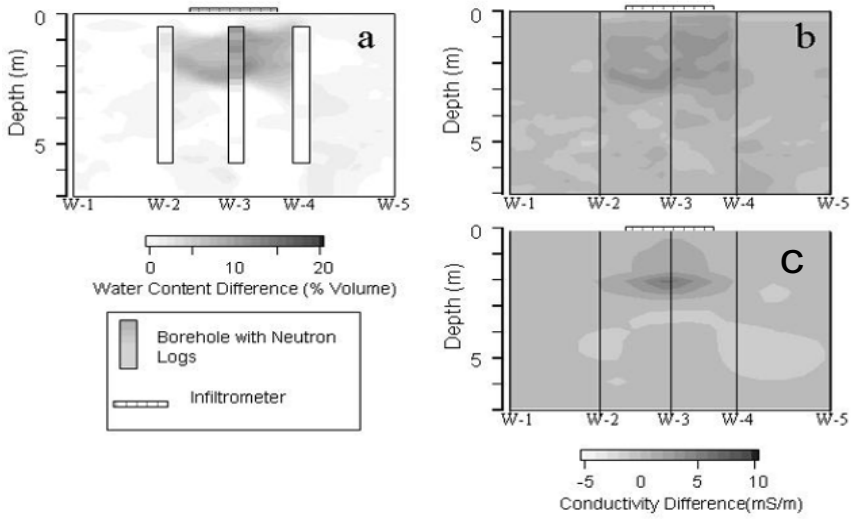

Figure 14.15. Images of (a) the change in volumetric water content from GPR and borehole neutron data, (b) conductivity data from crosshole GPR attenuation, and (c) ERT data. Data were collected between March 18

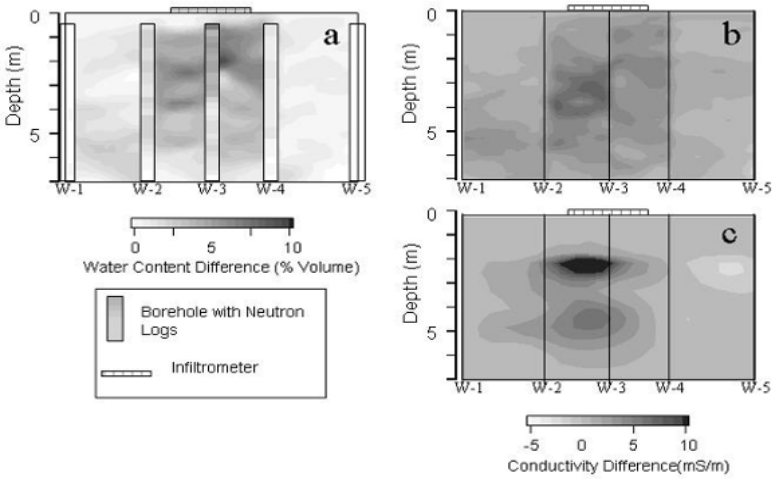

Figure 14.16. Images of (a) change in volumetric water content from GPR and borehole neutron data, (b) conductivity data from crosshole GPR attenuation, and (c) ERT data. The data were collected between April 20 and April 22, 1999, approximately 40 days after the start of infiltration.

After only 10 days of infiltration, the wetting front moved to a depth of about 2.5 m, as shown by the substantial increase in water content in the GPR images and neutron logs (Figure 14.15a). Unfortunately, because of the bentonite in the borehole annulus around W-3, the soil moisture content could not be accurately measured in the top meter of the borehole. The accuracy of the GPR was also limited in the upper meter, since there was a tendency for much of the signal to propagate up and along the air-earth interface rather than through the soil. Taking these limitations into account, the methods all show very similar results. Both neutron and GPR velocity images show a roughly tabular layer of increased moisture content about 2.5 m below the infiltrometer. The ERT and GPR attenuation images show a similar increase in conductivity corresponding to the zone of increased water content. None of the methods indicates that the infiltrating water has moved horizontally away from the infiltrometer.

After 40 days of infiltration (Figure 14.16), the images and the apparent movement of water are more complex. GPR moisture content images show more extensive lateral movement of the wetting front than is apparent in the neutron logs. The conductivity images from GPR attenuation (Figure 14.16b) data and the ERT data (Figure 14.16c) show somewhat similar features, but there are discrepancies in the magnitude and depth of the anomalies. Both GPR and ERT show strong increases in conductivity at shallow depths slightly southeast of the infiltrometer, and a deeper zone of modestly increased conductivity around 5 m extending almost to the boundary of the image region. GPR tends to show these two features as one continuous dipping layer; ERT shows them as a pair of distinct zones. In the GPR images, the anomalous conductive zones are slightly deeper than the zones of increased water content apparent in the neutron logs; in the ERT, they tend to be shallower. The ERT images agree fairly well with the site geology derived from soil cores that shows distinct layers at these two depths (Figure 14.16). The large differences in the GPR attenuation images always seem to fall between the large changes in moisture content. The GPR moisture content image and ERT image agree better than the ERT and GPR attenuation. It appears that GPR attenuation imaging is less robust than the velocity imaging, especially for tracking changes over time. Because the ERT represents an average that extends beyond the plane, it probably gives a better view of the overall large-scale processes on the site, whereas the GPR provides a better view of the complex local processes below the infiltrometer.

In summary, the geophysical methods in this study showed that the infiltration followed a complex path, moving rapidly downward through the coarse-grained layers, collecting and moving laterally within the finer-grained clay-bearing layers. All of the methods correlated well with each other. ERT data were able to provide fully 3-D images of the conductivity structure, which correlated well with changes in moisture content. This is probably because moisture is a volumetric parameter and ERT is a volumetric measurement. GPR data showed superior resolution to the ERT, but the results were limited to two-dimensional images along a single plane.

14.6 Conclusions

The studies presented in this chapter illustrated the use of many different geophysical methods for improving vadose zone characterization and monitoring. Resistivity (ERT), electromagnetic induction, and GPR methods are the primary tools for investigating the vadose zone, since they are the most sensitive of all of the conventional geophysical methods (excluding NMR and neutron-neutron scattering methods) to changes in water saturation. As was discussed in Chapter 1 of this volume, there is a natural ambiguity in using any single geophysical method to investigate the hydrogeologic properties in the vadose zone, and the use of multiple methods helps to confirm the location of major variations in the distribution of moisture.

The tank model study illustrated the sensitivity of GPR to subtle changes in the water saturation, and showed how 3-D mapping can provide valuable information concerning the distribution of regions of higher water saturation in pockets of higher water compaction. In addition, this study shows the complexities of using GPR to define the water table, since the geophysical water table determined by GPR is often different from the hydraulic water table defined in an observation well.

The potential of mapping soil water content in the presence of a varying water table using electrical measurements was discussed in Section 14.3.1, and the volumetric water content estimated from GPR groundwave studies in Section 14.3.2. These studies further illustrate the sensitivity of electrical conductivity and dielectric constant to soil water content.

Experimental results were shown that examine the changes in moisture content of soils due to natural loading as inferred from resistivity measurements. In one case study, surface resistivity arrays were used to monitor the spatial variability of infiltration resulting from snowmelt in a small field plot in Norway. In the second case study, borehole electrode arrays were utilized to monitor small changes in moisture content to a depth of 10 m at a site in a sandstone aquifers.

The studies at the STVZ site illustrate the use of crosshole GPR and ERT methods to infer or estimate the amount of water infiltration in the vadose zone. Although electrical conductivity is a function of a number of variables, its spatial pattern tended to be very strongly correlated to changes in moisture content within the vadose zone. Infiltrating water was observed to move rapidly through intervening sand and gravel layers, and tended to accumulate in clay-bearing layers. The changes as indicated in a qualitative sense by the geophysical images showed substantial lateral movement of the infiltrating water, illustrating that the infiltrating water moved beyond the image regions within a few months of the start of the experiment.

Each of the geophysical methods applied in this study, including the borehole methods, has strengths and weaknesses. The greatest strengths of ERT are its ability to monitor 3-D changes in moisture inferred from changes in electrical conductivity, and its ability to detect small changes in subsurface electrical properties. The method can be adapted to a range of scales; thus, the images in this study could be made from boreholes placed at

convenient distances around the periphery of the site. As such, the method has less resolution than the techniques to which it was compared.

The cross-borehole GPR method provided very good comparisons with other techniques. Allowing for the differences in resolution of the methods, the GPR-velocity-derived images of moisture content showed similar values to results obtained with the calibrated neutron data. Electrical conductivity derived from GPR attenuation data also showed patterns similar to both the EM-39 logs and the ERT-derived conductivities.

Overall, these case studies illustrate a broad range of geophysical methods that can be applied to detecting and monitoring variations in vadose zone electrical properties. These studies also serve to illustrate that geophysical measurements provide an indirect means to monitor changes in hydraulic properties, and should always be interpreted in light of local geologic variations.

Acknowledgments

Jeff Daniels and Barry Allred would like to acknowledge funding support from the USDA, EPA, and technical Support Unit of Region V. They are grateful for the dissertation work of Changryol Kim (which was supported by the USEPA) and give special thanks to Mark Vendl, Jim Ursic, and Steve Ostrodka of the USEPA for their continued support of environmental testing. David Alumbaugh and Doug LaBrecque would like to acknowledge the Department of Energy's Environmental Science Program, and Lee Paprocki for collecting the field data and doing the lab analysis. Andrew Binley acknowledges financial support from the UK Natural Environment Research Council (Grant GR3/11500) and the UK Environment Agency for the sandstone vadose zone study. Field assistance to Binley was provided by Peter Winship at Lancaster University. The snowmelt study was carried out with assistance from Helen French and Leif Jakobsen (Agricultural University of Norway) and Peter Winship and Carol Hardbattle (Lancaster University).

References

Abdul, A.S., Migration of petroleum products through a sandy hydrogeologic system, *Ground Water Monitoring Review, 8*(4), 73–81, 1988.

Alumbaugh, D., L. Paprocki, J. Brainard, and C.A. Rautman, Monitoring infiltration within the vadose zone using cross borehole ground penetrating radar, *Proceedings of the Symposium on the Application of Geophysics to Engineering and Environmental Problems*, 273–281, Environmental and Engineering Geophysical Society, Wheat Ridge, Colorado, United States, 2000.

Alumbaugh, D., P.Y. Chang, L. Paprocki, J.R. Brainard, R.J. Glass, and C.A. Rautman, Estimating moisture contents using cross-borehole ground penetrating radar: A study of accuracy and repeatability in context of an infiltration experiment, Tentatively Accepted by *Water Resour. Res.*, 2002.

Banton, O., M. K. Seguin, and M. A. Cimon, Mapping field-scale physical properties of soil with electrical resistivity, *Soil Sci. Soc. Am. J., 61*, 1010–1017, 1997.

Bedient, P.B., H.S. Rifai, and C.J. Newell, *Ground Water Contamination*, Prentice Hall, Englewood Cliffs, New Jersey, 1994.

Benderitter, Y., and J.J. Schott, Short time variation of the resistivity in an unsaturated soil: The relationship with rainfall, *European J. Env. Eng. Geophys., 4*, 37–49, 1999.

Binley, A. and K. Beven, Vadose zone flow model uncertainty as conditioned on geophysical data, *Ground Water, 41*(2), 114–127, 2003.

Binley, A., P. Winship, R. Middleton, M. Pokar, and J. West, High resolution characterization of vadose zone dynamics using cross-borehole radar, *Water Resour. Res., 37*(11), 2639–2652, 2001.

Binley, A., P. Winship, L.J. West, M. Pokar, and R. Middleton, R., 2002a, Seasonal variation of moisture content in unsaturated sandstone inferred from borehole radar and resistivity profiles, *J. Hydrology, 267*, 160–172, 2002a.

Chang, P., D. Alumbaugh, J. Brainard, and L. Hall, The application of ground penetrating radar attenuation tomography in a vadose zone infiltration experiment, Submitted to *Journal of Contaminant Hydrology*, 2003.

Doolittle, J.A., K.A. Sudduth, N.R. Kitchen, and S.J. Indorante, Estimating depths to claypans using electromagnetic induction methods, *J. Soil and Water Cons., 49*(6), 572–575, 1994.

Doolittle, J., M. Petersen, and T. Wheeler, Comparison of two electromagnetic induction tools in salinity appraisals, *J. Soil and Water Cons., 56*(3), 257–262, 2001.

Du, S. Determination of water content in the subsurface with the groundwave of ground penetrating radar, PhD-Thesis for Ludwig-Maximilians-Universität, München, Germany, 1996.

Eigenberg, R.A., and J.A. Nienaber, Electromagnetic survey of cornfield with repeated manure applications, *J. Environ. Qual., 27*, 1511–1515, 1998.

Fraisse, C.W., K.A. Sudduth, and N.R. Kitchen, Delineation of site-specific management zones by unsupervised classification of topographic attributes and soil electrical conductivity, *Trans. ASAE, 44*(1), 155–166, 2001.

French, H.K., C. Hardbattle, A. Binley, P. Winship, and L. Jakobsen, Monitoring snowmelt induced unsaturated flow and transport using electrical resistivity tomography, *J. Hydrology, 267*, 273–284, 2002.

Frohlich, R.K. and C.D. Parke, The electrical resistivity of the vadose zone—Field survey, *Ground Water, 27*(4), 524–530, 1989.

GeoTom, LLC, *User Mannual for GeotomCG and GeoTom3D*, 1998.

Grote, K., S.S. Hubbard, and Y. Rubin, Field-scale estimation of volumetric water content using GPR groundwave techniques, *Wat. Resour. Res. 39*(11), 1321, 10.1029/2003WR002045, 2003

Kean, W.F., M.J. Waller, and H.R. Layson, Monitoring moisture migration in the vadose zone with resistivity, *Ground Water, 27*(5), 562–561, 1987.

Hendrickx, J.M.H., B. Baerends, Z.I. Rasa, M. Sadig, and M. Akram Chaudhry, Soil salinity assessment by electromagnetic induction of irrigated land, *Soil Sci. Soc. Am. J., 56*, 1933–1941, 1992.

Hubbard, S.S., K. Grote, and Y. Rubin. Mapping the volumetric soil water content of a California vineyard using high-frequency GPR groundwave data, *Leading Edge of Expl. 21*, 552–559, 2002.

Huisman, J.A., and W. Bouten, Accuracy and reproducibility of measuring soil water content with the groundwave of ground penetrating radar. *J. of Env. and Eng. Geophysics 8*(2), 65–73, 2003a.

Huisman, J.A., S.S. Hubbard, J.D. Redman, and A.P. Annan, Measuring soil water content with ground penetrating radar: A review, *Vadose Zone Journal, 4*(2), 476–491, 2003b.

Huisman, J.A., J.J.J.C. Snepvangers, W. Bouten, and G.B.M. Heuvelink, Mapping spatial variation in surface soil water content: Comparison of ground-penetrating radar and time domain reflectometry, *J. of Hydrol. 269*, 194–207, 2002.

Huisman, J.A., J.J.J.C. Snepvangers, W. Bouten, and G.B.M. Heuvelink, Space-time characterization of soil water content: Combining ground-penetrating radar and time domain reflectometry, Accepted by *Vadose Zone J.,* 2003.

Huisman, J.A., C. Sperl, W. Bouten, and J.M. Verstraten, Soil water content measurements at different scales: Accuracy of time domain reflectometry and ground-penetrating radar, *J. of Hydrol., 245*, 48–58, 2001.

Inman, D.J., R.S. Freeland, J. T. Ammons, and R. E. Yoder, Soil investigations using electromagnetic induction and ground penetrating radar in southwest Tennessee, *Soil Sci. Soc. Am. J.*, *66*, 206–211, 2002.

Kim, C.R., A physical model experiment on the hydrogeologic applications of GPR, Ph.D. Dissertation, The Ohio State University, 2001.

Kravchenko, A.N., G.A. Bollero, R.A. Omonode, and D.G. Bullock, Quantitative mapping of soil drainage classes using topographical data and soil electrical conductivity, *Soil Sci. Soc. Am. J., 66*, 235–243, 2002.

Jackson, M.J., and D.R. Tweeton, 3DTOM: Three-dimentional geophysical tomography, *Report of Investigations 9617*, Bureau of Mines, United Stated Department of the Interior, 1996.

Jaynes, D.B., J. M. Novak, T. B. Moorman, and C. A. Cambardella, Estimating herbicide partition coefficients from electromagnetic induction measurements, *J. Environ. Qual., 24*, 36–41, 1995.

LaBrecque, D.J., and X. Yang, Difference inversion of ERT data: A fast inversion method for 3D *in situ* monitoring, *Journal of Environmental and Engineering Geophysics, 5*, 83–90, 2001.

LaBrecque, D.J., and Casale, Experience with anisotropic inversion for electrical resistivity tomography, *Proceedings of the Symposium on the Application of Geophysics to Engineering and Environmental Problems* (SAGEEP) '02, 2002.

Lesch, S.M., J.D. Rhoades, L.J. Lund, and D.L. Corwin, Mapping soil salinity using calibrated electronic measurements, *Soil Sci. Soc. Am. J., 56*, 540–548, 1992.

Paprocki, L., Characterization of vadose zone in-situ moisture content and an advancing wetting front using cross-borehole bround penetrating radar, Masters Thesis, New Mexico Institute of Mining and Technology, 2000.

Peterson, J.E., Pre-inversion correction and analysis of radar tomographic data, *Journal of Environmental & Engineering Geophysics, 6*, 1–18, 2001.

Sasaki, Y., Resolution of resistivity tomography inferred from numerical simulation, *Geophysical Prospecting, 40*, 453–464, 1992.

Scanlon, B.R., J.G. Paine, and R.S. Goldsmith, Evaluation of electromagnetic induction as a reconnaissance technique to characterize unsaturated flow in an arid setting, *Ground Water, 37*(2), 296–304, 1999.

Simms, J.E., and F.D. Morgan, Comparison of four least-squares inversion schemes for studying equivalence in one-dimensional resistivity interpretation, *Geophysics*, *57*(10), 1282–1293, 1992.

Sheets, K.R., and J.M.H. Hendrickx, Noninvasive soil water content measurement using electromagnetic induction, *Water Resour. Res., 31*(10), 2401–2409, 1995.

Topp, G.C., J.L. Davis, and A.P. Annan, Electromagnetic determination of soil water content: Measurements in coaxial transmission lines, *Water Resour. Res., 16*(3), 574–582, 1980.

Wharton, R.P., G.A. Hazen, R.N. Rau, and D.L. Best, Advancements in electromagnetic propagation logging, *Paper SPE 9041*, Society of Petroleum Engineers of AIME, Rocky Mountain Regional Meeting, 1980.

Zhou, Q.Y., J. Shimada, and A. Sato, Three-dimensional spatial and temporal monitoring of soil water content using electrical resistivity tomography, *Water Resour. Res.*, 37(2), 273–285, 2001.